Global nighttime lightning flash rates and characteristics observed with the FORTE satellite

T.E.L. Light[1], S.M. Davis[2], W. Boeck[3] and A.R. Jacobson[1]

[1]Space and Atmospheric Sciences Group, Los Alamos National Laboratory, Los Alamos New Mexico

[2] Laboratory for Atmospheric and Space Physics, University of Colorado, Boulder Colorado

[3] Niagara University, Niagara University New York

NOTE: This is a draft copy, intended for submission to the Journal of Geophysical Research, July 2003.

Short title: NIGHTTIME LIGHTNING FLASH RATES

Abstract. We estimate the FORTE/PDD detection efficiency for lightning flashes to be 62%, through comparison with TRMM/LIS observations of storms simultaneously viewed by both platforms. Using this value, we then examine the global lightning flash rate for nighttime lightning using 5 years of FORTE/PDD data. We find a nighttime land-ocean contrast in lightning activity of 4:1, and a global lightning flash rate of 81 flashes/second. We find that lightning over ocean appears to be somewhat more energetic optically than that over land, and we discuss two possible causes for this observation. Global lightning flash rates peak in August driven solely by the increase over land – the oceanic rate is constant throughout the year.

1. Introduction

A standard number for how much lightning occurs on the earth at any given moment (100 flashes/second) was first estimated nearly 80 years ago (*Brooks* [1925]), but it is only with the advent of satellite monitoring have we become able to quantitatively probe the intricacies of exactly when and where lightning occurs, on a global scale. The question is not merely academic. For example, *Williams* [1992] showed that on local scales, the rate of lightning activity appears sensitively correlated with wet-bulb temperature, and therefore a potentially useful monitoring tool for climate studies. Additionally, it is widely thought that lightning is a significant source of tropospheric reactive nitrogen oxides, which are important for atmospheric ozone chemistry (*Bond et al* 2002; *Tie et al.* 2002). The recent work by *Christian et al.* [2003] offers the most comprehensive view of global lightning rates to date. That work begins with a brief

review of prior estimates of global lightning activity, and proceeds to use five years' worth of data from the Optical Transient Detector, on board MicroLab-1 satellite, to measure lightning flash rate densities over the globe with high spatial resolution.

This current work similarly uses five years' worth of data, from the FORTE satellite Photodiode Detector. The FORTE satellite was jointly launched by Los Alamos and Sandia National Laboratories in 1997, and carries both radio frequency and optical detectors that monitor global lightning activity. This work differs significantly from the OTD study in three major ways. Firstly, our spatial resolution is limited to 1200 km on the ground. Secondly, the triggering mechanisms of the two instruments are different, and therefore each is likely subject to unique biases. Thirdly and most significantly, we consider only nighttime lightning data, for the reasons outlined below in section 2.3. This work is therefore not to be precisely compared to the OTD results, as lightning rates show significant diurnal variations, which themselves vary geographically.

2. FORTE Photodiode detector data

The FORTE Optical Lightning System includes a fast, broadband photometer, the Photodiode Detector, or PDD. The PDD employs a noise-riding-threshold trigger to record 1.92 ms optical waveforms of events with 15 μs resolution, and is sensitive from 0.4 to 1.1 μm. The field-of-view of the instrument is an 80° cone, or 40° maximum nadir angle. From FORTE's 825-km orbit, this results in a $\sim$ 1200-km-diameter footprint on the ground. For greater detail, see *Kirkland et al.* [2001] and *Suszcynsky et al.* [2000, 2001]. Waveforms from the PDD display a wide variety of characteristics; a given

waveform may show a single optical pulse or several, and pulses have a very large range of signal-to-noise. An example of the variety present in PDD waveforms is shown in Figure 1 which shows a selection of data recorded on July 1, 1998.

2.1. PDD particle event filter

The FORTE database of PDD events contains a flag that indicates whether the waveform for a given event is likely to have resulted from an impact on the detector by a high energy particle. Such impacts cause brief PDD signals which are not dispersed through cloud and are consequently extremely narrow ($< 75\mu$s). The database flags such narrow events, and for the flash rate density estimates in this work we exclude them. It is possible that, in so doing, our filter either flags a significant percentage of lightning-like events as bad, or it fails to flag a significant percentage of particle hits. In an effort to quantify the efficacy of the filter, and to gain confidence in using it, we examined by eye approximately 5,000 individual waveforms that were collected over the South Atlantic Anomaly (SAA) between June-December 1998, plus another 5,000 waveforms gathered over the rest of the globe. In the global set, 0.14% of all events were flagged as particle hits when in fact they were lightning, and no true particle hits were missed by the filter. In the SAA data, 0.02% of all events were flagged as particle hits when in fact they were lightning, and 2.8% of so-called lightning was in fact due to particle hits. Thus we believe our filter to work very well, with the worst miss-rates being less than 3% and only over the SAA.

2.2. PDD detection efficiency

We determined the PDD total lightning flash detection efficiency through comparison with that of the Lightning Imaging Sensor (LIS) on board the NASA/TRMM satellite. There are a very limited number of coincident TRMM/FORTE overpasses of a given geographic region, due to the large difference in orbital inclination between the two satellites. We have nevertheless identified two times when both satellites were in view of the same region, and an active storm was present. These storms are examined in detail by *Boeck et al.* [2003].

Each flash, as reported by LIS, is composed of several (2 - 200) events, with total flash durations from a few milliseconds up to 1-2 seconds. As the FOV for the two satellites is not precisely coincident, it is possible that some PDD records originate from a flash entirely outside the storm viewed by LIS. To prevent such contamination and consequent over-estimation of our flash-level detection efficiency, we visually inspected both the LIS and PDD data for each flash, and accepted only those PDD events which were within 4 ms of a LIS event.

The first storm occurred at -13.2° north latitude and 48.1° east longitude on April 5, 2001, at approximately 12:30 a.m. local time. LIS was in view of the storm for 86 seconds, in which time 32 flashes were observed. The FORTE/PDD was enabled and in view for 6 of these flashes. Using the procedure described above, we found PDD detections for all 6 of them. The second, and more active, storm occurred at 26° north latitude and -92° east longitude on September 20, 2001, at approximately 12:15 a.m.

local time. LIS observed the storm for about 96 seconds, and detected 76 flashes. FORTE was in view of the storm for only the final 21 of these flashes, and detected 13 of them.

The LIS nighttime detection efficiency is estimated to be $93 \pm 4\%$, and the gross 24-hour DE is estimated to be $88 \pm 9\%$ (*Boccippio et al.* [2002]), although those authors state that these are likely overestimates. We therefore use the more conservative value of 88%, and find that the PDD detection efficiency 19/27 of the LIS DE, or 62%. The limitations of this estimate are many. Firstly, it is based on observations of only two storms, for a total of three minutes. Secondly, both of these storms occurred over ocean. The PDD is a threshold-crossing detector, and is more sensitive to higher peak amplitude waveforms, whereas the LIS is an integrating detector. The lightning-type distribution varies geographically such that there is a greater fraction of intracloud lightning over ocean (e.g., *Mackerras et al.* [1998]; *Boccippio et al.* [2000a]), and IC lightning typically shows weaker-amplitude waveforms with longer duration than those from cloud-to-ground lightning (*Light et al.* [2001a]; *Davis et al.* [2002]). It is therefore possible that the PDD detection efficiency is higher over land, where a greater fraction of CG lightning occurs.

There is one final caution regarding the PDD detection efficiency derived above. The PDD field-of-view is nominally $\pm 40^\circ$ but in fact has a gentle roll-off such that beyond 40° the detection does not drop immediately to zero. The number of flashes seen by LIS that we believe were in FORTE's FOV and therefore detectable by the PDD depends on what cutoff we use for the FOV. The solid curve in Figure 2 shows

how the final calculated PDD flash detection efficiency depends on our choice of FOV. In this work, we will use 40° for a PDD DE of 62%. The reader can scale the results with a higher or lower detection efficiency using the solid curve in Figure 2. Also shown in Figure 2 is the stroke-level detection efficiency of the PDD: 19% relative to LIS, using a 40° FOV.

2.3. Limitations of the data

One fundamental limitation in the present study is that the PDD does not provide geolocation of a detected event apart from the event's being in the satellite's FOV. We are limited with this data set to geographic resolution of 1200-km-diameter on the ground.

Additionally, during daylight observations, the operating trigger thresholds are set high to avoid having the data contaminated by glints off clouds or water. Due to these high trigger thresholds, in addition to the high daytime background light levels, the PDD data taken during daylight are extremely biased and include only the strongest optical lightning events. That is, the daytime PDD data preferentially sample cloud-to-ground lightning, whereas the nighttime data offer a distribution more representative of the fraction of weak, in-cloud lightning (*Light et al.* [2001a]; *Davis et al.* [2002]). In this work we therefore exclude the $\sim$ 10% of data taken during daylight conditions, and consider only nighttime PDD data. With nighttime data we probe lightning more deeply within the distribution of peak power outputs. Figure 3 illustrates this point by comparing the conditional probabilities of peak and integrated power from two years of

PDD daytime and nighttime data.

3. Flash Rate Determination

In this section we describe how we derive the two components of our flash rates – namely, the number of flashes in a given region during a given period of time, and the fraction of that time period in which the PDD was configured to collect data, over that region. The final flash rate is then the number of flashes in a given region divided by the observation time there, and scaled by the area of the region and the DE. We calculate flash rate maps with 0.5° resolution, and then coarsen that to 5° for the final product. Any 5° region that PDD observed for less than 5 minutes is considered as unobserved, and no rate is assigned to that grid cell.

3.1. View time determination

We begin by searching the FORTE state-of-health files to find all the times when the PDD was in the desired configuration. The sub-satellite position at each such second of time is noted. From each sub-satellite point, we determine the PDD footprint on the ground, and all the 0.5° grid cells falling within that footprint receive one second of time. In this way, we create a map of how much time the FORTE/PDD could detect lightning from any given point on the Earth.

The desired configuration for the FORTE PDD is defined to be all times when *(i)* the sensor was on, *(ii)* event storage was enabled, *(iii)* event detection was enabled, *(iv)* the PDD was triggering autonomously (rather than being slaved to the other optical

lightning sensor on FORTE), and *(v)* the trigger threshold levels were set to 25 digitizer levels or less (the lowest setting, typical of nighttime observations).

3.2. Defining a flash

Once a map of the global observation time is generated, we search the database for all PDD events recorded when the sensor was in the configuration described above. We then reject any events that fail a procedure to classify them as lightning. The procedure rejects events that are likely to be energetic particle hits as described in section 2.1 (see *Kirkland et al.* [2001] for a detailed description of the particle filter).

All good events are then grouped into flashes. A flash, as defined by LIS, incorporates a 333-ms sliding window between subsequent pulses as well as a spatial requirement that subsequent pulses be within 15 km of one another (*Christian et al.* 2000). We do not have geolocation information for the PDD data but we wish nevertheless to define a flash as closely as possible to the LIS definition. A complication arises in that the PDD stroke level detection efficiency, as described above, is 19% relative to LIS. That is, on average the PDD will see only one fifth of the strokes which would make up a single LIS flash. Missing events will widen the temporal gap between subsequent detected events in the same flash, such that it is possible for the PDD to report seeing two or more flashes where LIS would only have reported one. Therefore to determine the optimal sliding window for use with PDD data, in order that on average one LIS flash will be counted also as a single PDD flash, we perform the following simple simulation.

Using the 108 flashes detected by LIS in the two storms described above (section 2.2), we found the distributions of inter-event spacing and the number of pulses in a flash. We then constructed contrived flash-length temporal records for 7500 flashes, such that the distributions of simulated pulse separation and flash multiplicity approximated the observations. For each of these simulated flashes, we randomly selected 19% of the events that PDD would observe, and constructed a new time series of pulse separations. Finally, we determined how many flashes would appear to arise from each parent flash, for a given sliding window used by the PDD to define a flash grouping. The distributions used in the simulation and the results are shown in Figure 4. If the window is too small, the missed events cause gaps that artifically break a parent flash into multiple PDD flashes. The relative PDD/LIS flash ratio levels off below unity because with a 19% stroke level DE, there will unavoidably be some flashes the PDD fails to detect. From this simple simulation, it appears that a sliding window of 436 ms is optimal for statistically reproducing LIS flashes with the PDD's lower stroke-level detection efficiency. If all PDD events occurred at constant interval with a period smaller than 436 ms, the data would result in a few extremely long flashes. But because flashes really are temporally isolated and finite, however, that does not happen and in fact we see few flashes lasting longer than 1 second. As an example, Figure 5 shows the distribution of derived flash durations using the sliding 436 ms window.

The mean sub-satellite point and time of all events constituting a flash is used to determine the satellite's observational footprint at the time of each flash. Each 0.5° grid cell within the footprint is then incremented by one flash. Figure 6 shows the PDD data

for a representative flash that occurred 1 July 1998.

Using this flash definition we can also determine an average intra-flash event rate for each flash, which is simply the number of PDD events constituting a given flash, divided by the PDD-determined duration of the flash. Figure 7 shows the distribution of intra-flash event rates determined in this way. This can only be done for flashes with at least two events. There is a maximum detectable rate of two events per ~ 2.5 ms (the nominal time for the PDD to re-arm between successive records), or 0.4 evt/ms. That is, flashes with event rates of $\sim$0.4 evts/ms were triggered with a suspicious regularity. We often see this occur when the PDD triggers repeatedly off of glint due to a particular alignment of the sun, satellite and sea surface, and we therefore have excluded from the data the approximately 0.4% of flashes that show evidence of this pattern.

4. Global Flash Rates

Plate 1 shows the global lightning flash rate density derived from PDD data as described above, for five years' worth of data, from 1998-2002. In order to highlight the low-flash-density regions of the globe, the color scale is logarithmic in the lower panel. Despite the 1200 km resolution of the data, we clearly see the continental lightning "hot spots" along the equator, as well as the marked land-ocean contrast in lightning flash density. 2,020,883 PDD events grouped into 515,346 flashes (excluding those due to repeated glint triggers) are contained in this map. Table 1 lists some of the coarse statistics for these data. We consider four data groupings – global, "equatorial" (referring to data located within 40° of the equator), data over land and data over ocean.

Table 1. Flash-rate-density statistics from 5 years (1998-2002) of data.

	Global	Equatorial ($\|\text{lat}\| \leq -40^\circ$)	Over Land (all lats)	Over Ocean (all lats)
mean flashes/year/km^2	5.0	7.7	9.5	2.3
mean # flashes/sec[1]	81	125	154	37
median flashes/year/km^2	1.3	3.5	5.4	0.8
median # flashes/sec[1]	21	57	87	13

[1]These values result from extrapolating a *global* flash rate from each regional flash rate density.

In addition to measuring simply when and where a flash occurred, we can use the FORTE PDD data to examine a few characteristics of those flashes. For example, we can measure the peak power observed from a flash, and the total observed flash energy. We must point out, however, that the PDD record of a flash is a series of snapshots that does not capture the flash in its entirety. Therefore the peak power, energy and duration of flashes, as observed by the PDD, are to be considered lower limits. For the 19 flashes jointly observed by TRMM/LIS and FORTE/PDD, Figure 8 compares the peak power and total energy measured by PDD with the LIS-reported radiance for the flash, showing that all these measures of the flash energetics are proportional. Table 2 compares flash characteristics over land and ocean, for the overall PDD observations.

Table 2. Land/ocean flash characteristics. Mean and median values from 5 years (1998-2002) of data.

Region	Flash peak power (μW/m^2)	Total flash energy (μJ/m^2)	Flash duration (ms)	Flash event rate (#/ms)
Land mean values	24,300.	1.8	353	0.033
Ocean mean values	51,700.	3.0	344	0.034
Land median values	200	0.30	256	0.017
Ocean median values	232	0.33	253	0.017

4.1. Monthly variation of global flash characteristics

We examined five years' worth of data sorted into months to investigate annual variations in the lightning flash rate. Therefore data from five Januarys, five Februarys, et cetera, combine to give us monthly flash rate maps. From these, we calculate the mean flash rates as shown in Figure 9. There is a slight trend for lightning rates to increase through the second and third quarters of the year over land and the "equatorial" regions, but the oceanic rate is quite constant. Consequently, the ratio of land-to-ocean lightning flash rates is also very constant for half the year, but begins to rise in northern summer as shown in Figure 10. The ratio peaks in September, coincident with the highest lightning flash rates of the year, occurring over South America in the autumn (see plate 2). The average land-to-ocean ratio is 4.2.

There is no significant monthly variation seen in any of the following quantities:

flash duration, peak power, integrated energy, stroke rate, or the number of events comprising a flash.

4.2. Seasonal variation of global flash characteristics

Plate 2 shows the global flash rate density for each of four seasons. Each season includes three months, for five years, so that a total of 15 months of PDD data is combined to make each map. As a result the spatial sampling is quite good, except for the southernmost extent of the South American Anomaly (SAA). We often shut off FORTE's optical sensors over the SAA to minimize the memory waste caused by very high rates of energetic-particle hits.

In plate 2 the seasonal north-south shift of lightning activity is clear. Also obvious is the fact that the highest lightning flash rates are seen over the Amazon between September and November. Rates there can exceed 100 flashes per sq. km per year. However, the most continually active region is Central Africa, which keeps a fairly steady rate of ~ 60 flashes per sq. km per year.

5. Regions of Interest

We next consider the flash rates and flash characteristics in several regions distributed around the globe, as shown in Figure 11. We define 5 regions over land, 6 over ocean and 2 coastal regions (the Indonesian archipelago and the United States Gulf Coast). Table 3 compares median values of the flash rate densities and flash characteristics for these 13 regions. We use the median values because the distributions

of flash characteristics are highly skewed, and the median is therefore more representative of the population than is the mean. Nevertheless, it appears that while lightning occurs more frequently over land masses, the lightning flashes that do occur in the oceanic regions contain a greater fraction of energetic events.

Table 3. Regional flash characteristics. Median values from 5 years (1998-2002) of data.

Region	**Flash rate density (fl/yr-km^2)**	Flash peak power (μW/m^2)	Total flash energy (μJ/m^2)	Flash duration (ms)	Lat/ Lon Ranges
		Continental regions			
N. America	**2.5**	224	0.34	258	35→ 50; -120→ -90
S. America	**24.5**	208	0.29	259	-23→ 0; -68→ -45
N. Africa	**5.0**	158	0.23	268	15→ 30; 0→30
S/Cent. Africa	**28.6**	195	0.31	256	-25→ 5; 15→ 30
Asia	**2.4**	168	0.19	246	30→ 45; 60→ 105
		Oceanic regions			
N. Pacific	**1.3**	216	0.28	235	15→ 45; -175→ -150
S. Pacific	**2.0**	230	0.33	248	-45→ -15; -170→ -140
E/Equ. Pac.	**2.1**	273	0.39	264	-10→ 10; -120→ -90
N. Atlantic	**2.3**	235	0.33	258	30→ 45; -55→ -25
S. Atlantic	**0.29**	369	0.48	248	-45→ -15; -30→ 0
Indian Ocean	**0.51**	251	0.31	281	-40→ -15; 70→ 100
		Land/ocean regions			
U.S. Gulf Coast	**19.6**	249	0.35	261	23→ 38; -105→ -75
Indonesia	**15.0**	219	0.33	259	-20→ 10; 105→ 135

6. Comparison to previous work

Direct comparison of these results to other lightning flash-rate studies is complicated by FORTE biases, and in particular by the use of nighttime-only data. A few comments are nevertheless appropriate. The most similar study is that of *Christian et al.* [2003], in which the NASA Optical Transient Detector was used to measure global flash-rate densities over a five year period. Their instrument is an imaging CCD with $\sim$ 10km spatial resolution. That system triggers after energy within a 2ms integration exceeds threshold, whereas the FORTE/PDD triggers when an individual 15 μsec sample exceeds threshold. Thus our system is somewhat biased against triggering on low-amplitude, temporally-extended events, which the OTD will more easily detect. Further, the OTD is operated even during daylight, with reduced (but characterized) detection efficiency (*Boccippio et al.* 2002). Nevertheless, some comparisons are appropriate, with the caveat that diurnal variability of the geographic distribution of lightning will preclude exact comparability of results. Table 4 lists the several statistics measured by both the OTD study and this present work, for comparison.

In addition to the *Christian et al.* [2003] OTD study, other authors similarly find an order-of-magnitude contrast in the land-ocean lightning flash rates (see e.g., *Boccippio et al.* 2000b or *Williams et al.* 2002, and references therein).

Table 4. Comparison of global flash rate statistics from OTD and FORTE studies.

	Forte finding	OTD finding
Global flash rate (flashes/sec)	80	44
Land-to-ocean ratio	4	10
Maximum annual flash rate density (fl-km^2-yr^{-1})	~ 58	~ 80
Location of max. annual flash-rate density	Central Africa	Kemembe, Rwanda
Oceanic temporal rate variability	constant	constant
Continental temporal rate variability	peaks in August	peaks in August

7. Conclusions

Through comparison with data from LIS, we have estimated the FORTE/PDD flash detection efficiency to be $\sim 62\%$. Uncertainties in our final flash rates are largely driven by the uncertainty of this value. We find an overall mean global flash rate of 81 flashes/second.

Using FORTE/PDD data, we have constructed global maps of lightning flash rate density, in which are seen all the same high- and low- flash-rate regions as seen in previous studies of lightning activity worldwide. However, we find a land-ocean contrast in lightning rates of 4:1, whereas previous estimates find continental lightning to be a full order of magnitude more frequent than that over ocean. This we attribute to a diurnal effect, wherein lightning over land quiets at night to a greater extent than over ocean. Indeed, *Williams et al.* [2000] found that the total lightning flash counts over

land differed from the total global counts by a roughly constant fraction, at all local hours. This argues that the flash counts over ocean (the global - land difference) is roughly constant over 24 hours, whereas the land value is sharply peaked in the late afternoon. In a study limited to the eastern Mediterranean, *Altaratz et al.* [2003] found that the ratio of CG:IC lightning peaked at 13:00 local time over land, but at 5:00 local time over ocean. Combined with the fact that ground flashes tend to be the most optically bright, as observed by FORTE (*Light et al.* 2001a), this suggests that the overall satellite-based detection of global flash rates may be biased to seeing oceanic lightning at night, and continental lightning during the day.

Tables 2 and 3 show that oceanic lightning flashes appear to be more energetic, as observed from space, than land lightning. A similar finding was reported by *Boccippio et al.* [2000b] from OTD and LIS data. More specifically, the mean peak power and total energies of lightning flashes appear to be a factor of 2 greater over ocean than over land in the FORTE data. The median values, however, differ by only 10-15%, suggesting that the lightning optical energy distributions are in fact similar over land and ocean, but with a slightly larger tail of extreme events in the oceanic distribution. There is a radio frequency analog to this effect: the radio frequency sensors on board FORTE routinely observe extremely powerful VHF pulses due to the attachment process occurring over seawater (*Jacobson & Shao* 2002). Alternatively, the statistical appearance of more extreme optical events over ocean may simply be due to a difference in the cloud cover (scattering medium) over ocean; more tenuous cloud layers would allow a greater fraction of light emitted below the cloud to escape to the satellite (see e.g., *Light et al.*

2001b or *Thomason & Krider* 1982).

Examination of the temporal variation of lightning activity shows that flash rates increase throughout the second and third quarters of the year over land (April - September), while oceanic rates remain constant. The single highest rate observed is $\sim$ 100 flashes/km^2/yr, occurring between September and November over the Amazon region of Brazil. Central Africa is the only region of continually sustained high lightning rates ($\sim$ 60 flashes/km^2/yr) throughout the year. We observed no apparent monthly or seasonal variation in the optical characteristics of lightning flashes.

Acknowledgments. The authors would like to thank the entire FORTE Science and Operations team at Los Alamos Laboratory and at Sandia Laboratory for useful discussions regarding the FORTE sensors and data. This work was supported by the U.S. Department of Energy.

References

Altaratz, O., Z. Levin, Y. Yair & B. Ziv, Differences in winder lightning over land and sea across the eastern coast of the Mediterranean, in *Proceedings of the 12th International Conference on Atmospheric Electricity*, S. Chauzy & P. Laroche (Eds.), ONERA, Paris, France, 2003.

Boccippio, D.J., K.L. Cummins, H.J. Christian & S.J. Goodman, Combined Satellite- and Surface-Based Estimation of the Intracloud-Cloud-to-Ground Lightning Ratio over the Continental United States, *Monthly Weather Review, 129*, 108-122, 2000a.

Boccippio, D.J., S.J. goodman & S. Heckman, Regional differences in tropical lightning distributions, *Jour. App. Meteor., 39,* 2231-2248, 2000b

Boccippio, D.J., W.J. Koshak, & R.J. Blakeslee, Performance Assessment of the Optical Transient Detector and Lightning Imaging Sensor. Part I: Predicted Diurnal Variability, *J. Atmos. Oceanic Tech., 19*, 1318-1332, 2002.

Boeck, W.L., A.R. Jacobson, H.J. Christian & S.J. Goodman, Multi-satellite observations of oceanic lightning, in *Proceedings of the 12th International Conference on Atmospheric Electricity*, S. Chauzy & P. Laroche (Eds.), ONERA, Paris, France, 2003.

Bond, D.W., S. Steiger, R.Y. Zhang, X.X. Tie & R.E. Orville, The importance of MOx production by lightning in the tropics, *Atmos. Environment, 36,* 1509-1519, 2002.

Brooks, C.E.P., The distribution of thunderstorms over the globe, *Geophys. Memo., 3*(24), 147-164, 1925.

Christian, H.J., R.J. Blakeslee, S.J. Goodman & D.M. Mach (Eds.), *Algorithm Theoretical Basis Document (ATBD) for the Lightning Imaging Sensor (LIS),* 53 pp., NASA/Marshall Space Flight Center, Alabama, 2000. (Available at

http://eospso.gsfc.nasa.gov/atbd/listables.html)

Christian, H.J., R.J. Blakeslee, D.J. Boccippio, W.L. Boeck, et al., Global frequency and distribution of lightning as observed from space by the Optical Transient Detector, *J. Geophys. Res., 108*, 4005, doi:10.1029/2002JD002347, 2003.

Davis, S.M., D.M. Suszcynsky & T.E. Light, FORTE observations of optical emissions from lightning: Optical properties and discrimination capability, *J. Geophys. Res., 107*, 4579-4583, 2002.

Jacobson, A.R. & X.M. Shao, FORTE satellite observations of very narrow radiofrequency pulses associated with the initiation of negative cloud-to-ground lightning strokes, *J. Geophys. Res., 107,* 4661, doi:10.1029/2001JD001542, 2002.

Kirkland, M.W., D.M. Suszcynsky,J.L.L. Guillen & J.L. Green, Optical observations of terrestrial lightning by the FORTE satellite photodiode detector, *J. Geophys. Res., 106*, 33499-33509, 2001.

Light, T.E., D.M. Suszcynsky & A.R. Jacobson, Coincident radio frequency and optical emissions from lightning, observed with the FORTE satellite, *J. Geophys. Res., 106*, 28,223-28,231, 2001a.

Light, T.E., D.M. Suszcynsky, M.W. Kirkland & A.R. Jacobson, Simulations of lightning optical waveforms as seen through clouds by satellites, *J. Geophys. Res., 106,* 17,103-17,114, 2001b.

Mackerras, D., M. Darveniza, R.E. Orville, E.R. Williams & S.J. Goodman, Global Lightning: Total, Cloud and Ground Flash Estimates, *Jour. Geophys. Res., 103*, 19791-19809, 1998.

Suszcynsky, D.M., M.W. Kirkland, A.R. Jacobson, et al., FORTE observations of simultaneous

VHF and optical emissions from lightning: Basic Phenomenology, *J. Geophys. Res., 105*, 2191-2201, 2000.

Suszcynsky, D.M., T.E.L. Light, J.L. Green, J.L.L. Guillen & W. Myre, Coordinated observations of optical lightning from space using the FORTE photodiode detector and CCD imager, *J. Geophys. Res., 106*, 17897-17906, 2001.

Thomason, L.W. & E.P. Krider, The Effects of Clouds on the Light Produced by Lightning, *J. of Atmos. Sci., 39,* 2051-2065, 1982.

Tie, X.X., R.Y. Zhang, G. Brasseur & W.F. Lei, Global NOx production by lightning, *Jour. Atmos. Chem., 43,* 61-74, 2002.

Williams, E.R., The Schumann resonance: A global tropical thermometer, *Science, 256,* 1184-1187, 22 May 1992.

Williams, E., K. Rothkin, D. Stevenson & D. Boccippio, Global lightning variations caused by changes in thunderstorm flash rate and by changes in the number of thunderstorms, *Jour. App. Meteor., 39*, 2223-2230, 2000.

Williams, E. & S. Stanfill, The physical origin of the land-ocean contrast in lightning activity, *C.R. Physique, 3*, 1277-1292, 2002.

Received _____

Figure 1. PDD waveforms recorded 1 July 1998. These data were selected to show the wide variety of waveform shapes observed in the 1.92 ms PDD records. The sub-satellite location is indicated above each waveform.

Figure 2. The derived PDD flash detection efficiency for a range of assumed values for the PDD field-of-view, which is nominally 40°. The numbers above each plot point indicate the number of LIS flashes contributing to the points. The dotted curve shows the stroke DE for the PDD relative to LIS.

Figure 3. Probability distributions for data taken in 1998/1999. The top panel shows the peak power density; the bottom panel shows the integrated energy density. In both panels, daytime and nighttime data are separated.

Figure 4. (a) The distribution of the number of pulses seen per LIS flash, for the 108 flashes observed in the storms also viewed by FORTE. The dashed curve shows the distribution of the number of pulses per simulated flash. (b) The distribution of average pulse separation for the 108 flashes observed by LIS in the storms also viewed by FORTE. The dashed curve shows the distribution of the average pulse separation for the simulated flashes. (c) The average number of PDD-determined flashes per LIS flash, as a function of the PDD sliding window size used to define a flash, using the 7500 simulated flashes with the multiplicity and pulse separation distributions shown in the dashed curves of panels (a) and (b).

Figure 5. The distribution of flash durations resulting from use of a 436 ms sliding window as described in the text, for all data from 1998-2002.

Figure 6. An example of an optical lightning flash as observed by the FORTE PDD. The lower panel shows the relative timing and power of the ten events comprising the flash, and also indicates the flash time and the sub-satellite location at the time of the event. The smaller, upper panels show the detailed PDD records for each of the ten events.

Figure 7. The distribution of intra-flash event rates derived as described in the text for all data from 1998-2002.

Figure 8. Comparison of the LIS-reported flash radiance with the total energy and peak power observed by the FORTE/PDD for each flash observed by both sensors. We have used the geolocation provided by LIS to estimate the at-source values from PDD data, assuming isotropic emission.

Figure 9. The mean lightning flash rate densities versus month, for five years worth of data. We have differentiated by region to give the global, "equatorial" ($|\text{lat}| \leq 40°$.), land and oceanic means. These global flash rates are calculated by extrapolating a regional flash rate densities over the globe.

Figure 10. The ratio of the mean land to ocean flash rate densities as a function of month.

Figure 11. The 13 regions considered individually in the text.

Plate 1. Lightning flash rate density in flashes per year per square kilometer, for the years 1998-2002. In the lower panel, the color scale is logarithmic to bring out the full range of features.

Plate 2. Lightning flash rate density in flashes per year per square kilometer, for each of four seasons, with a linear color scale. The data span five years, so that each map includes data from 15 months. The specific months contributing to a given season are noted in each map.

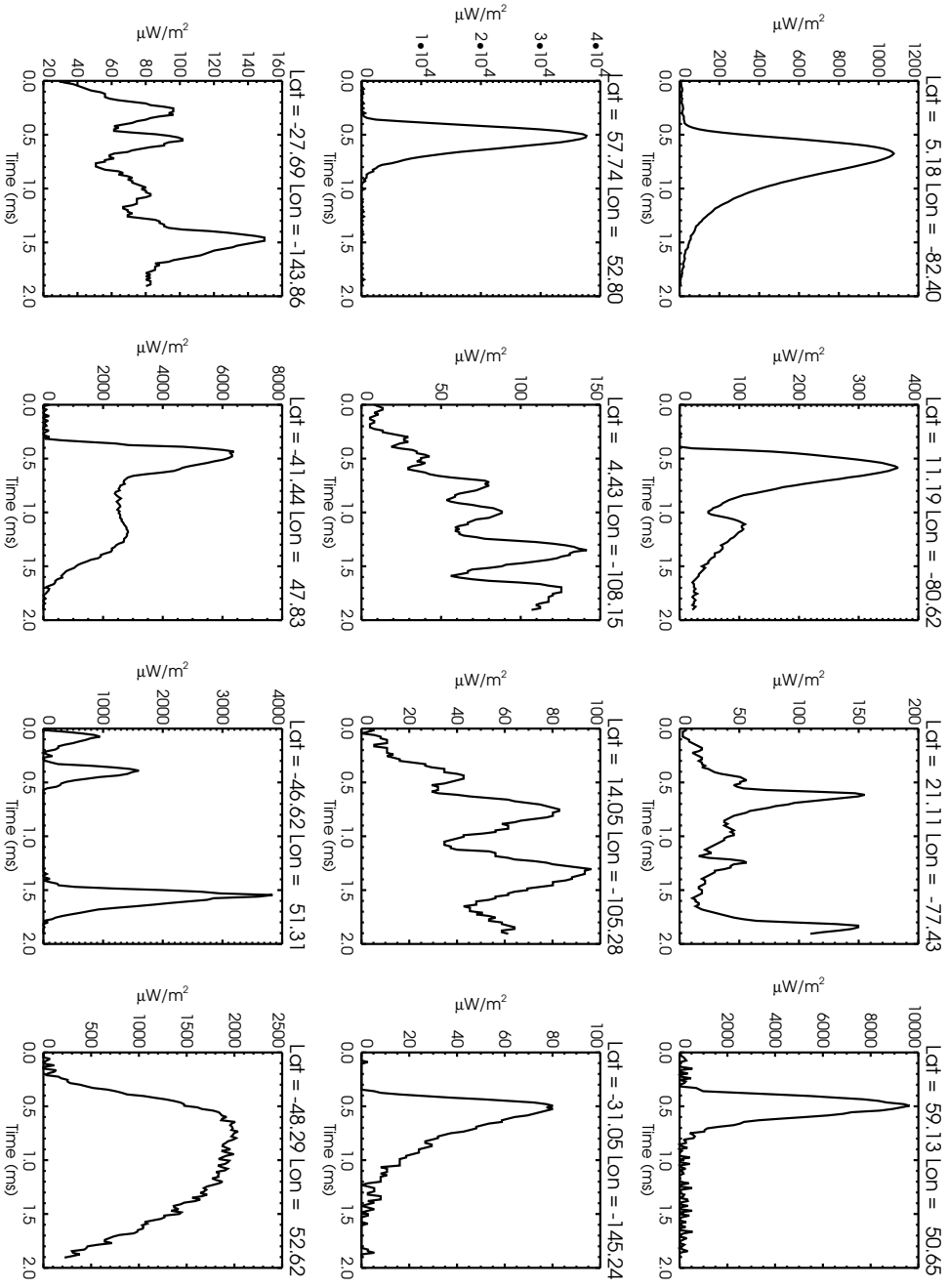
Lat = 59.13 Lon = 50.65
Lat = 21.11 Lon = -77.43
Lat = 11.19 Lon = -80.62
Lat = 5.18 Lon = -82.40
Lat = -31.05 Lon = -145.24
Lat = 14.05 Lon = -105.28
Lat = 4.43 Lon = -108.15
Lat = 57.74 Lon = 52.80
Lat = -48.29 Lon = 52.62
Lat = -46.62 Lon = 51.31
Lat = -41.44 Lon = 47.83
Lat = -27.69 Lon = -143.86
μW/m²
Time (ms)

Figure 1.

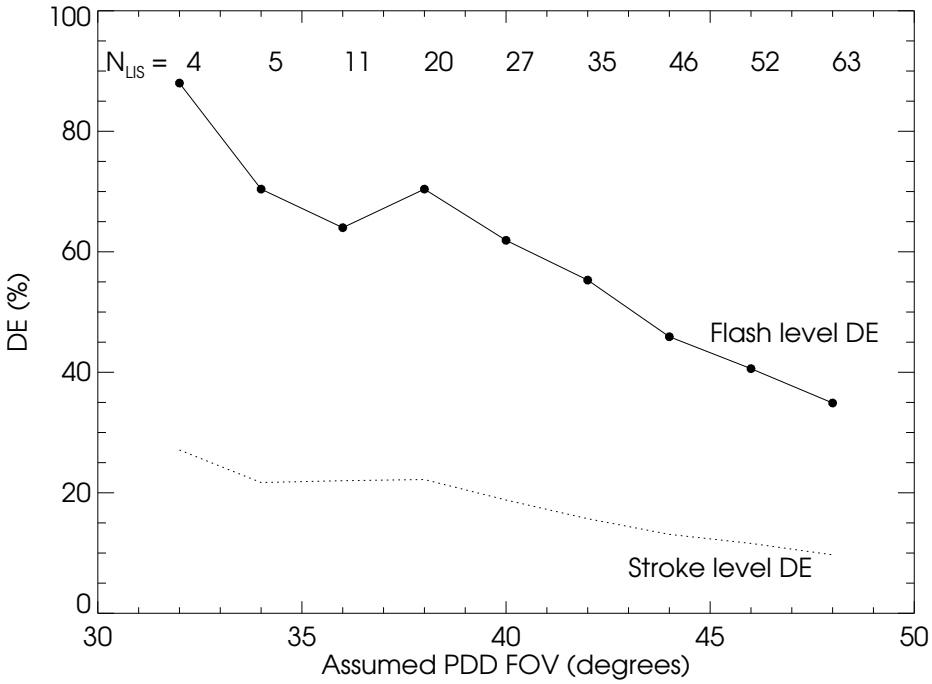
100
80
60
40
20
0
DE (%)
N_LIS = 4 5 11 20 27 35 46 52 63
Flash level DE
Stroke level DE
30
35
40
45
50
Assumed PDD FOV (degrees)

Figure 2.

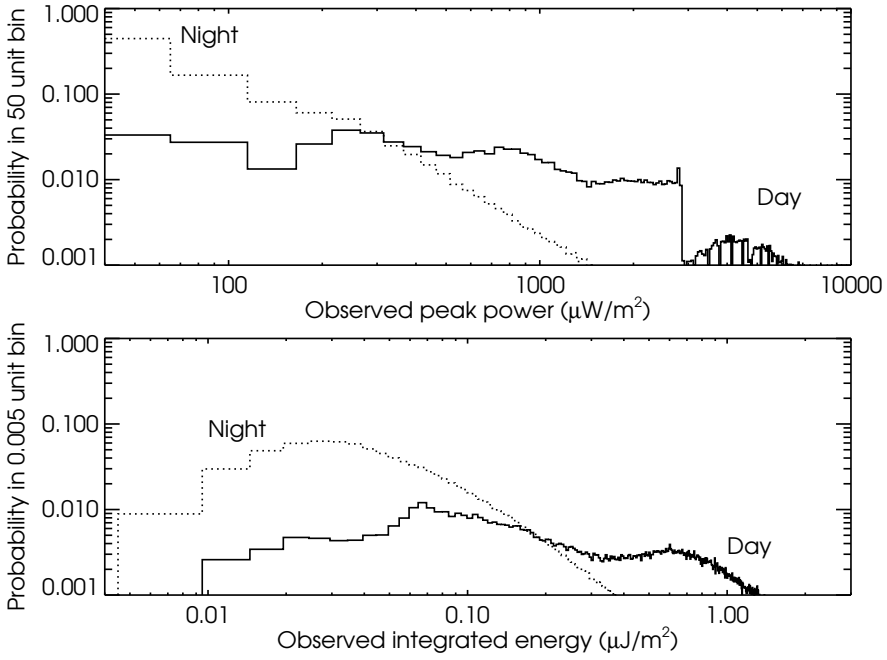
1.000
0.100
0.010
0.001
Probability in 50 unit bin
Night
Day
100
1000
10000
Observed peak power (μW/m²)
1.000
0.100
0.010
0.001
Probability in 0.005 unit bin
Night
Day
0.01
0.10
1.00
Observed integrated energy (μJ/m²)

Figure 3.

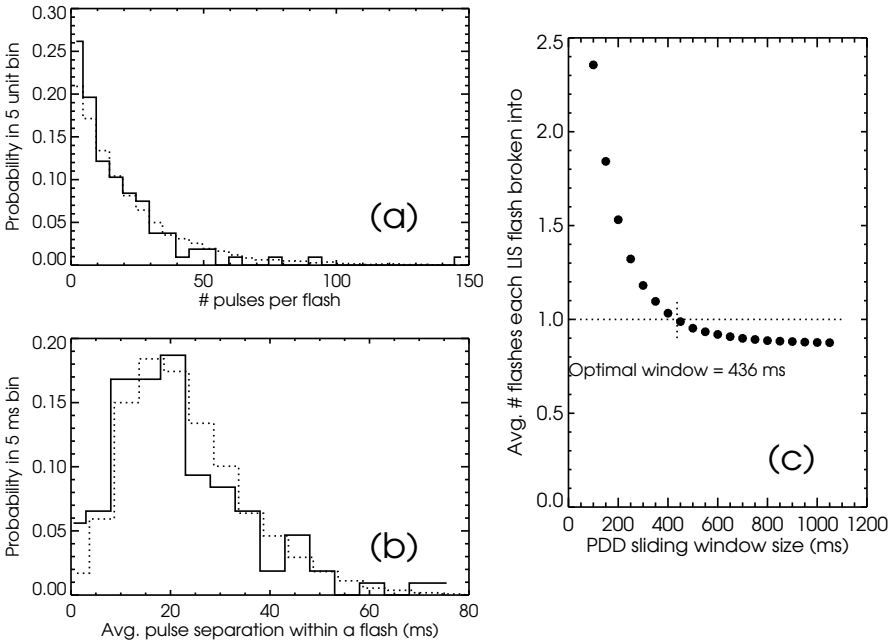
Probability in 5 unit bin
pulses per flash
(a)
Probability in 5 ms bin
Avg. pulse separation within a flash (ms)
(b)
Avg. # flashes each LIS flash broken into
PDD sliding window size (ms)
Optimal window = 436 ms
(c)

Figure 4.

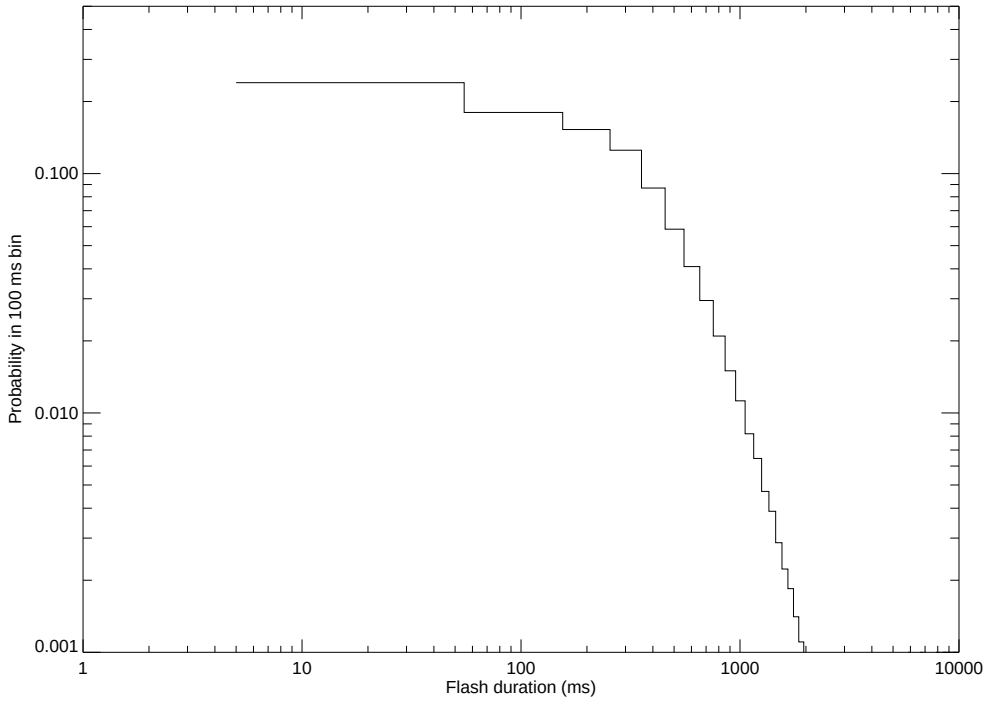
0.100
0.010
0.001
Probability in 100 ms bin
1
10
100
1000
10000
Flash duration (ms)

Figure 5.

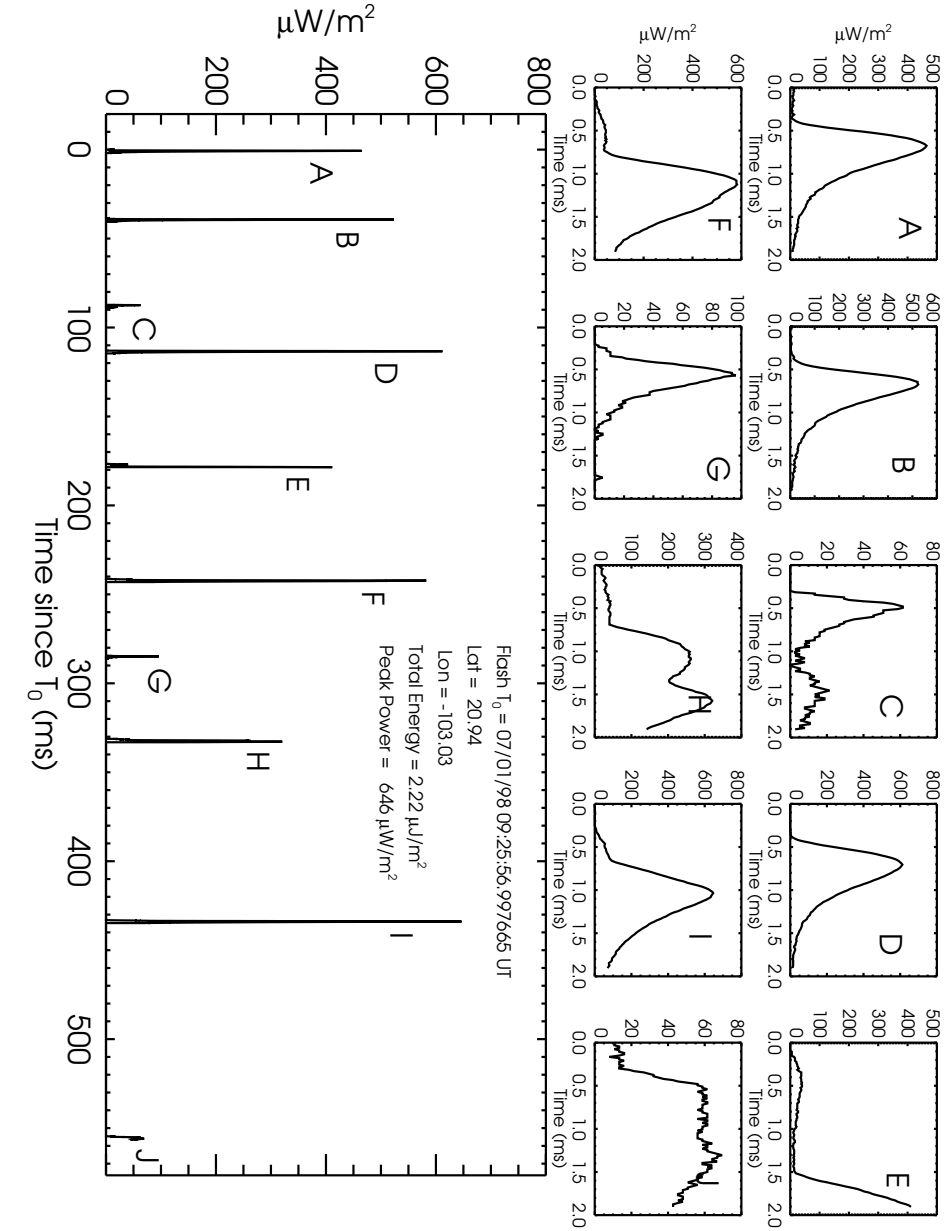
μW/m²
Time (ms)
A
B
C
D
E
F
G
H
I
J
Flash T0 = 07/01/98 09:25:56.997665 UT
Lat = 20.94
Lon = -103.03
Total Energy = 2.22 μJ/m²
Peak Power = 646 μW/m²
Time since T0 (ms)

Figure 6.

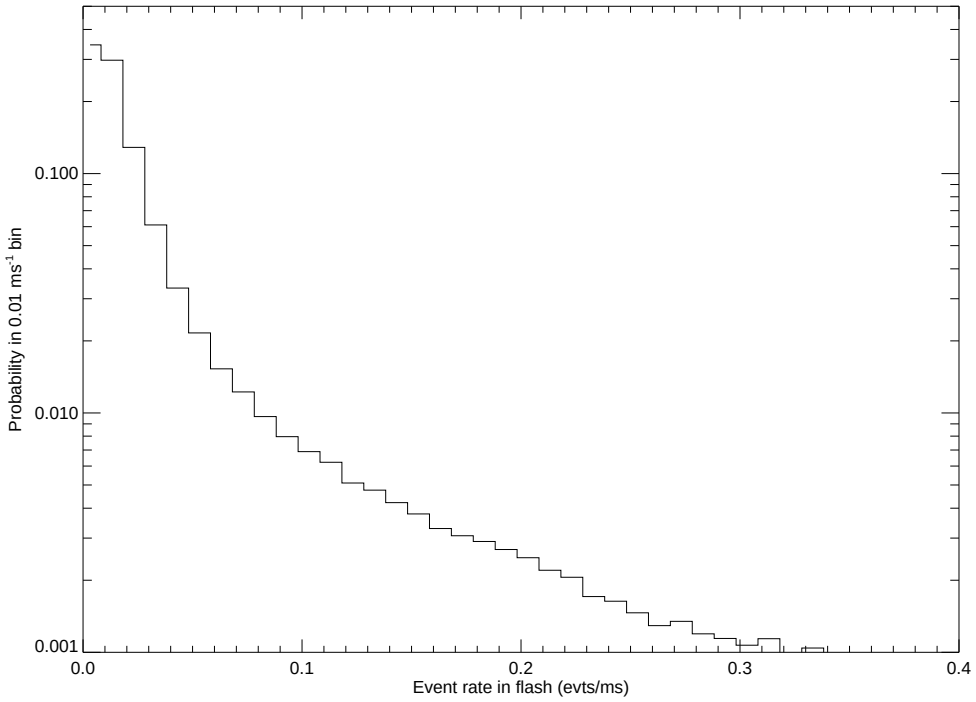
0.100
0.010
0.001
Probability in 0.01 ms^{-1} bin
0.0
0.1
0.2
0.3
0.4
Event rate in flash (evts/ms)

Figure 7.

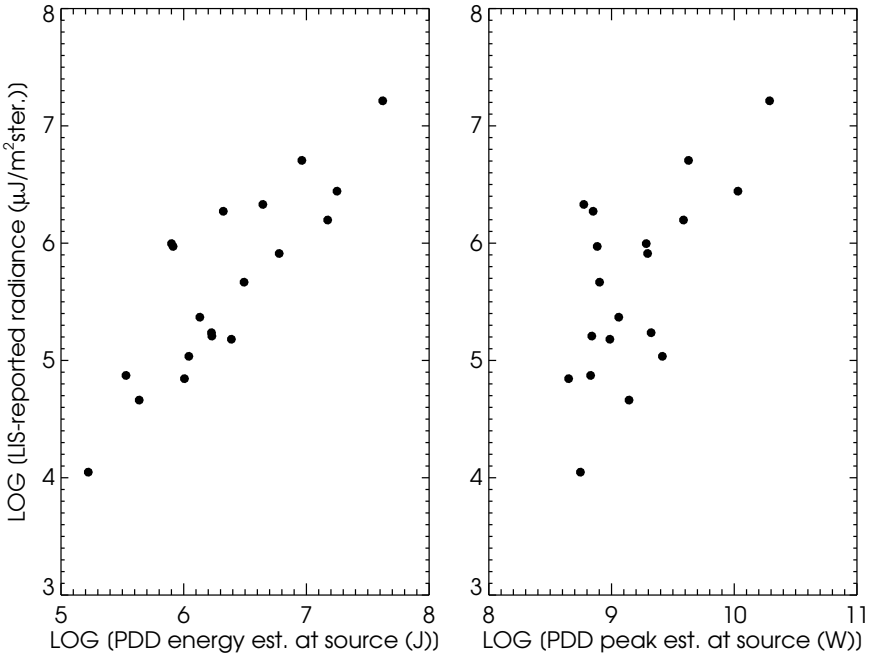
LOG (LIS-reported radiance (μJ/m²ster.))
LOG (PDD energy est. at source (J))
LOG (PDD peak est. at source (W))
3
4
5
6
7
8
9
10
11

Figure 8.

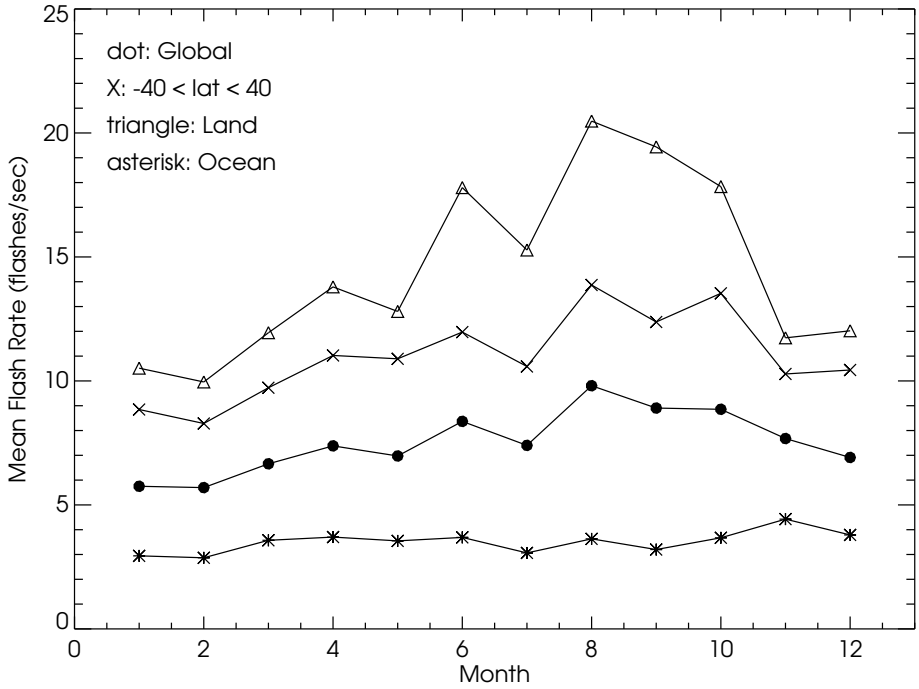
dot: Global
X: -40 < lat < 40
triangle: Land
asterisk: Ocean
Mean Flash Rate (flashes/sec)
Month
0
5
10
15
20
25
0
2
4
6
8
10
12

Figure 9.

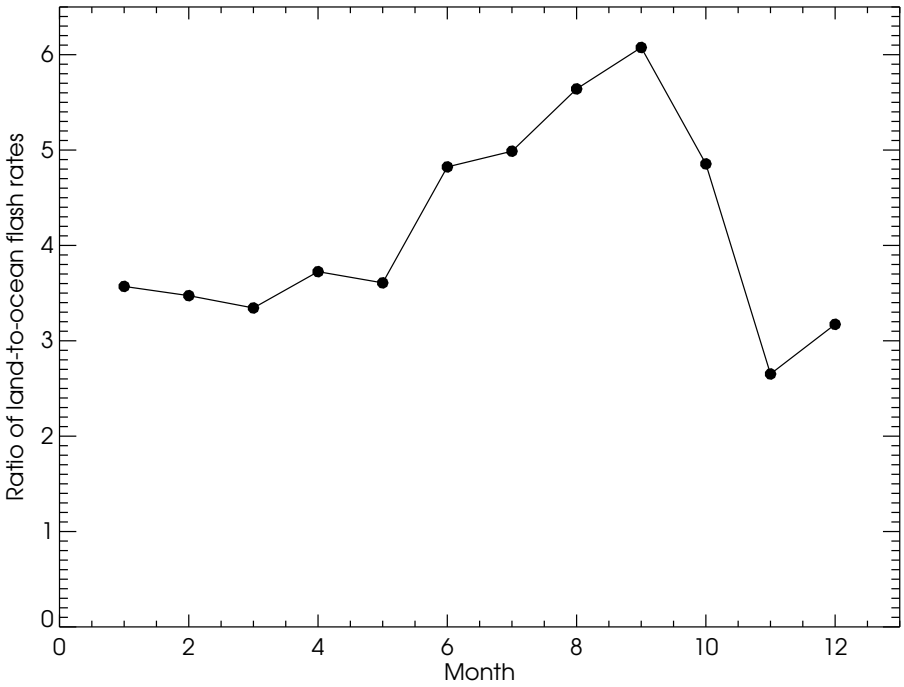

Figure 10.

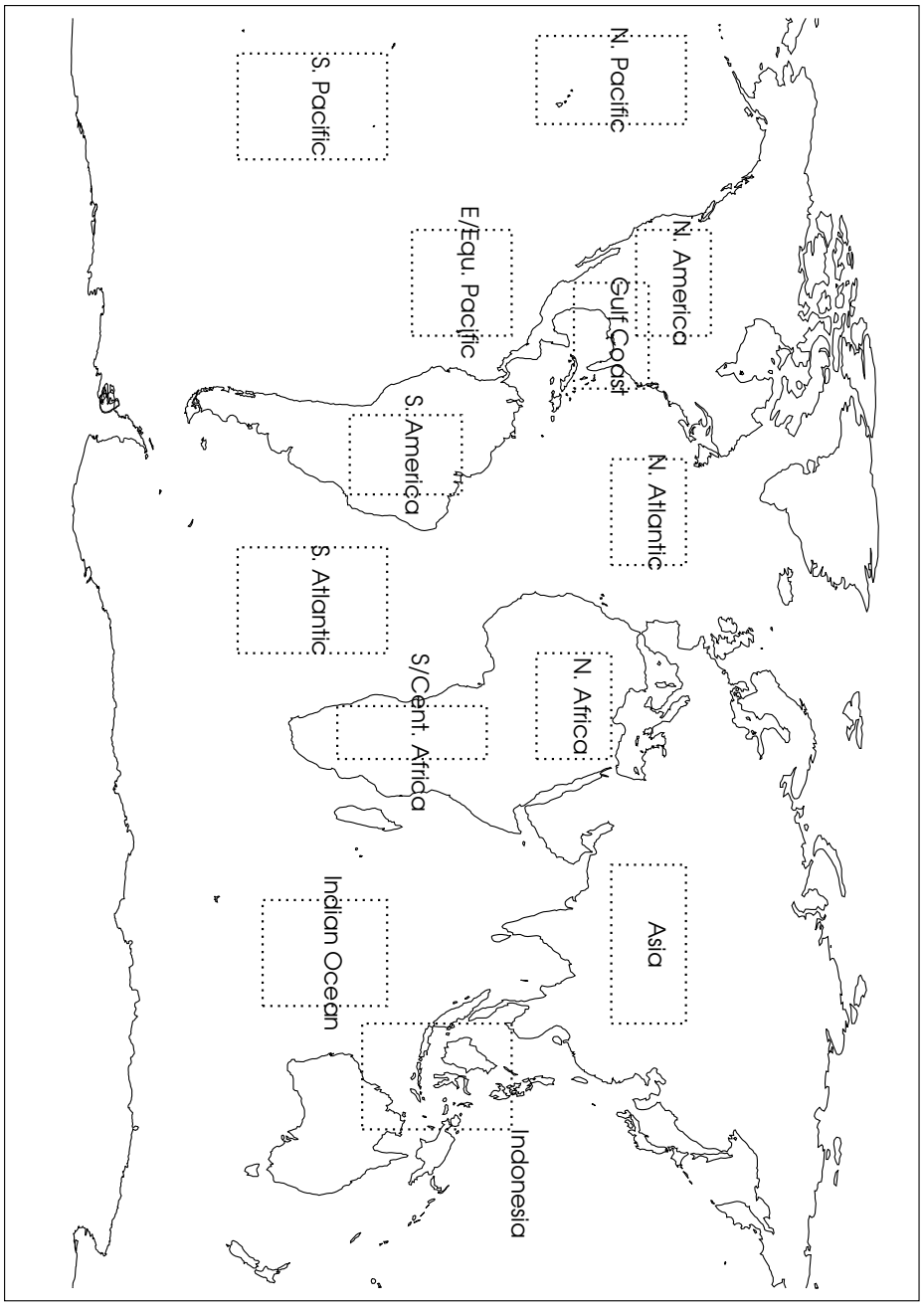
N. Pacific
S. Pacific
N. America
Gulf Coast
E/Equ. Pacific
S. America
N. Atlantic
S. Atlantic
N. Africa
S/Cent. Africa
Asia
Indian Ocean
Indonesia

Figure 11.

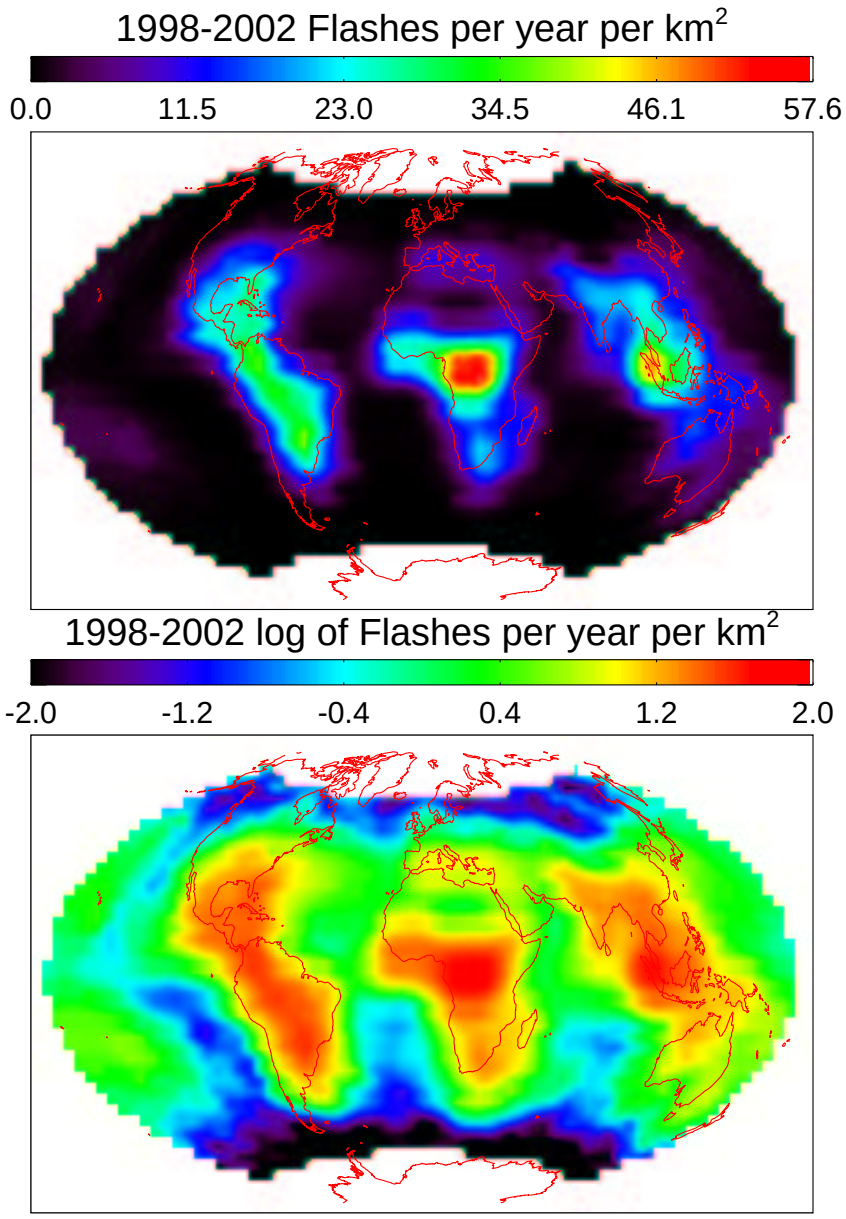
1998-2002 Flashes per year per km2
0.0
11.5
23.0
34.5
46.1
57.6
1998-2002 log of Flashes per year per km2
-2.0
-1.2
-0.4
0.4
1.2
2.0

Plate 1.

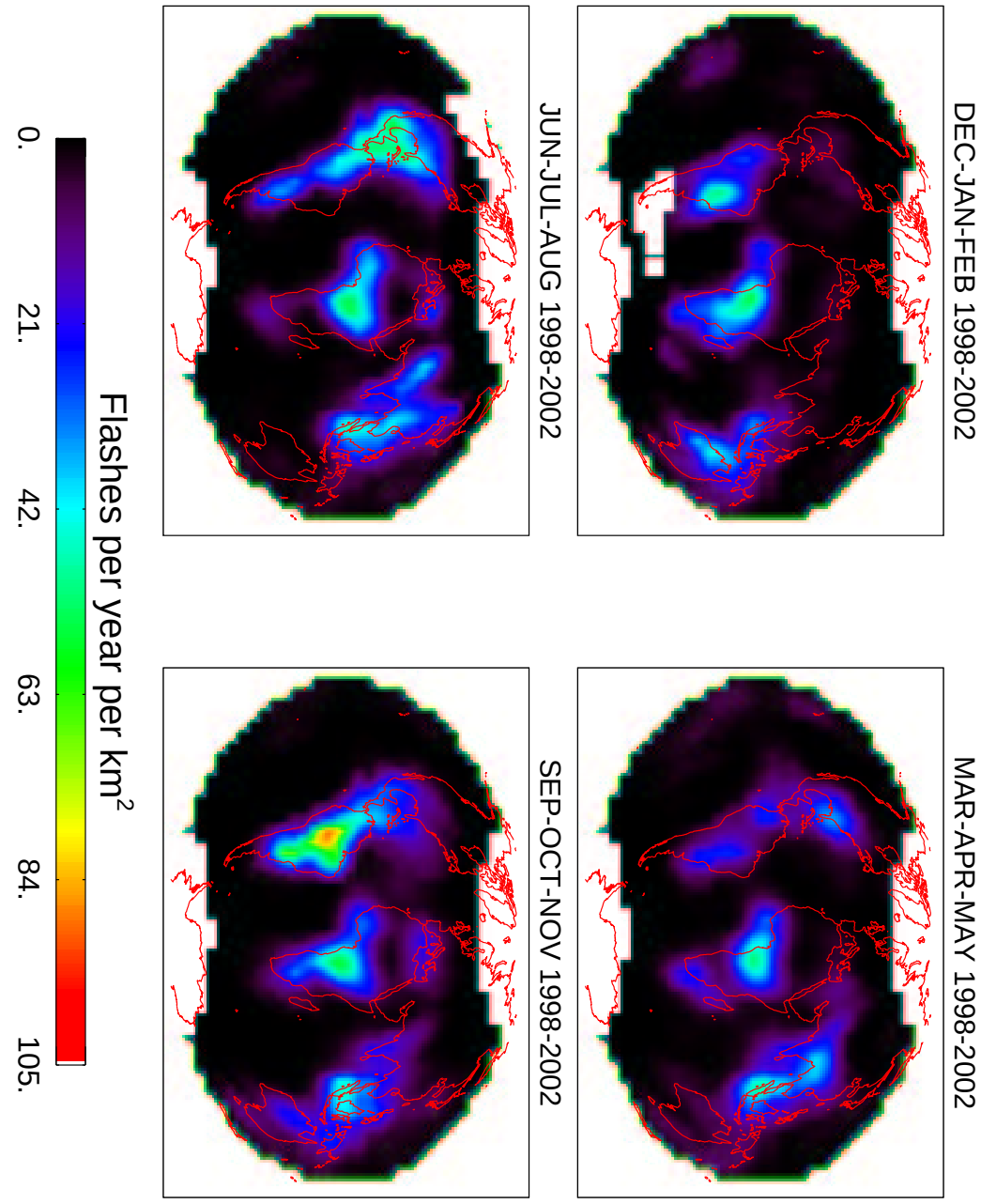
DEC-JAN-FEB 1998-2002
MAR-APR-MAY 1998-2002
JUN-JUL-AUG 1998-2002
SEP-OCT-NOV 1998-2002
Flashes per year per km^2
0.
21.
42.
63.
84.
105.

Plate 2.